Ceramics-Silikáty 66 (2), 157-166 (2022)
www.ceramics-silikaty.cz 10.13168/cs.2022.0010

EFFECT OF CRYSTALLISATION TEMPERATURE ON LAS TRANSPARENT GLASS-CERAMICS CONTAINING A HIGH Al_2O_3 CONTENT

MINGJUAN SHI, FENG HE#, ZHIQIANG ZHOU, XIAORONG YANG, JUNLIN XIE

State Key Laboratory of Silicate Materials for Architectures, Wuhan University of Technology, Wuhan 430070, PR China

#E-mail: he-feng2002@163.com

Submitted December 15, 2021; accepted February 14, 2022

Keywords: Low thermal expansion coefficient, β-quartz solid solution, the content of Al_2O_3, LAS transparent glass-ceramics

The influence of the crystallisation temperature on the structure and properties of Li_2O-Al_2O_3-SiO_2 (LAS) glass-ceramics with a high aluminium content was investigated. Glass-ceramics with ultra-low CTE and high transmittance were successfully prepared by the melt-quenching method and a two-step heat treatment. The crystallisation behaviour of the glass was studied via DSC and XRD. Besides, FTIR, Raman and FE-SEM were used to explore the structure of the samples under different crystallisation temperatures. The results showed that a β-quartz solid solution with nano-size precipitated from the glass after the heat treatment and when the crystallisation temperature was 820 °C, the bending strength and microhardness reached 156 MPa and 1082.09 HV, respectively.

INTRODUCTION

Glass-ceramics are formed by controlling the devitrification process inside the glass during the heat treatment [1]. The properties of such materials mainly depend on the type and faction of the crystalline phases precipitated in the glass [2]. Since glass-ceramics were invented by Stookey [3], different glass-ceramic categories have been developed. LAS glass-ceramics are widely utilised owing to the excellent thermal performance and transparency, which have been applied in the field of astronomical telescopes, cookware, tableware, 3D printing, etc. [4-6]. Many studies have been carried out on the glass-ceramics thermal expansion coefficient (CET), i.e., Venkateswaran et al. [7] prepared an LAS glass-ceramic with a CET of 3×10^{-7} K^{-1}. Soares [8] prepared LAS glass-ceramics with a CET of 0.2×10^{-7} K^{-1} by adjusting the heat treatment system. Al-Harbi et al. [4] prepared a porous LAS glass-ceramic with a controllable pore structure via gel injection moulding, and its CET was 0.11×10^{-7} K^{-1}.

Furthermore, high transmittance is also an important advantage of LAS glass-ceramics with a β-quartz solid solution as the main crystal phase. The main factors affecting the transmittance of a material are the optical scattering and particle absorption. For LAS glass-ceramics, the absorption is dominated by various transition metal ions in the residual glass whereas scattering comes from the precipitation of crystalline phases [9, 10]. The main crystal phase in this study regarding LAS glass-ceramics, a β-quartz solid solution, has a nano-grain size, resulting in the scattering of light at about 1/10 of the wavelength of visible light [6]. In addition, the determination of the heat treatment also has a significant influence on its transmittance. The grain size of the precipitated crystals can be controlled by adjusting the heat treatment schedule [11,12].

In the current research, there are few reports on the preparation of high transmittance as well as ultra-low expansion LAS glass-ceramics. In order to manufacture LAS glass-ceramics with these properties, the nano-sized β-quartz solid solution phase should mainly be obtained by adjusting the composition and heat treatment conditions. When the Al_2O_3 content is low, the lithium disilicate phase is more likely to be precipitated [12]. Moreover, only when the Al_2O_3 content is high, the β-quartz solid solution phase is easily precipitated [37], but it will transform to the β-spodumene solid solution with a larger grain size at higher temperatures [9]. In the optimal composition of transparent ultra-low expansion LAS glass-ceramics, the Al_2O_3 content is generally in the range of 17 ~ 24 wt. % [38], and the Al_2O_3 content in common commercial LAS transparent glass-ceramics is generally less than 25.5 wt. % [6].

However, there are not many studies on the Al_2O_3 content in which it is more than 25 wt.%. Zhao et al. [2] prepared mullite nanocrystalline glass-ceramics in which the transmittance reached 75 %, but its flexural resistance was not significant. In the low-expansion transparent LAS glass-ceramics prepared by Wu et al. [39], when the Al_2O_3 content reached the highest value (25.5 wt. %), its visible light transmittance was not high (< 70 %). Kumar et al. [13] prepared LAS glass-ceramics with a visible light transmittance of more than 80 %, but its thermal expansion coefficient showed a negative expansion only in the low temperature range, and the Al_2O_3 content was 25 wt.%. Zhang et al. [14] prepared a low-expansion transparent LAS nanocrystalline glass with a transmittance of 85 % (thickness of 1.2 mm) via thermoelectric treatment, and the Al_2O_3 content was 24 wt. %. Our previous research shows [9] that increasing the Al2O3 content will inhibit the transformation from a β-quartz solid solution to a β-spodumene solid solution, which is beneficial to obtain a smaller grain size, thereby improving the visible light transmittance of the glass-ceramics, so the Al_2O_3 content designed in this paper is 26 wt. %, and the LAS glass-ceramics with low expansion and high transmittance are prepared through the exploration of heat treatment conditions.

What is more, the Al_2O_3 content is generally in the range of 10 wt. % to 25 wt. % in the LAS glass-ceramics with the main crystalline phase of a β-quartz solid solution, and the research on LAS glass-ceramics with a high Al_2O_3 content (> 25 wt. %) have rarely been reported [9, 15, 16]. In this work, the innovation is the determination of the crystallisation temperature of LAS glass-ceramics with a high Al_2O_3 content (26 wt. %). Moreover, the LAS glass-ceramics treated at 820 °C for 2 h had good properties: high transmittance of 88 % in the visible wavelengths, low CET of -0.682×10^{-7} K^{-1} in the range of 30 – 500 °C, and the bending strength and microhardness reached to 156 MPa and 1082.09 HV, respectively. The results indicated that it is of great significance for broadening the application of LAS glass-ceramics in transparent kitchenware and optic devices.

MATERIAL AND METHODS

Preparation of parent glass

The parent glass within the chemical composition (wt. %) of 60 SiO_2, 26 Al_2O_3, 5 Li_2O, 1.573 TiO_2, 2.427 ZrO_2, 2 BaO, 2.5 ZnO, 0.5 Na_2O were obtained from analytical grade chemicals, Li_2O was introduced by Li_2CO_3, Al_2O_3 was introduced by $Al(OH)_3$, Na_2O was introduced by Na_2CO_3, and BaO was introduced by $BaCO_3$. The parent glass was melted at 1650 °C for 3 hours. After being formed on a 400 °C graphite heating plate, a glass block with a size of 40 mm × 40 mm × 25 mm was obtained. Then the formed block glass was placed in a muffle furnace at 550 °C for 2 h to eliminate the internal stress to obtain the parent glass. The parent glass was cut into multiple 4 mm × 4 mm × 4 mm glass strips by an internal cutting machine, and then treated in the muffle furnace, both the nucleation and crystallisation time were 2 h, the heating rate was 10 °C·min^{-1}.

Characterisation

Differential scanning calorimetry (DSC, STA449F3, NETZSCH) was used for the thermal analysis. After the parent glass was ground into a powder with a ball mill and passed through a 200-mesh sieve, a small part was taken in an Al_2O_3 crucible and heated from 25 to 1200 °C, the heating rate was 10 °C·min^{-1}. The glass-ceramics phase analysis was carried out by X-ray powder diffractometer (XRD, D8 Advance, Bruker), the scanning range was 10 – 80 °. The structure of the glass-ceramics was determined by Fourier transform infrared spectrometer (FTIR, Nicolet 6700, Thermo Electron Scientific Instruments) in a range of 200 – 2000 cm^{-1}. After polishing the glass-ceramic wafers, the transmittance was conducted by ultraviolet-visible spectrometer (Lambda 750 S, PerkinElmer) in a range of 200 – 800 nm, the thickness of the samples was 2 mm. The structure of the polished samples was tested by Raman spectrometer (Horiba Jobin Yvon, France). The microstructure of the glass-ceramics was examined by a scanning electron microscope (SEM, Zeiss Ultra Plus, Zeiss). The cross-section of the samples was polished and etched with 5 wt. % HF for 60 s, and then cleaned in an ultrasonic cleaner for 30 min. A thermal expansion meter was used to test the coefficient of thermal expansion (CET) of the samples (25 mm × 4 mm × 4 mm), the heating rate was 10 °C·min^{-1}. The three-point bending strength of the glass-ceramics was measured by a universal laboratory machine (AG-IC50KN, Shimadzu) with a span of 25 mm, the results were determined by calculating the average value of five samples. A Vickers microhardness tester (HVS-1000) was applied to measure the Vickers hardness of the glass-ceramics, the loading pressure and time were 1.98 N and 10 s, respectively. The samples were measured 12 times and averaged

RESULTS AND DISCUSSIONS

Thermal analysis

DSC analysis of parent glass

As shown in Figure 1, T_g is the glass transition temperature and T_c is the crystallisation temperature. The heat treatment schedule of the parent glass is usually designed according to the T_g and T_c [17]. The heat treatment included two steps: nucleation and crystallisation. The nucleation process was when

TiO_2 and ZrO_2 were added as the nucleating agents to promote the phase separation and self-nucleation in the glass forming process. The crystallisation increased the temperature on the basis of the nucleation to allow the crystal nuclei to grow and form large-sized crystals [18]. In this study, the influence of the crystallisation temperature and performance of high-Al_2O_3 LAS transparent glass-ceramics was discussed while keeping the nucleation temperature and time consistently. Crystal nuclei are usually precipitated ranging from 30 – 100 °C above the T_g [4]. T_g is 572 °C as shown in Figure 1, the nucleation temperature was chosen to be 600 °C. The crystallisation temperature was selected near the T_c [19]. Glass-ceramics with different crystallisation temperatures of 760, 780, 800, 820, 840 and 860 °C, marked as C-760, C-780, C-800, C-820, C-840 and C-860, respectively were used.

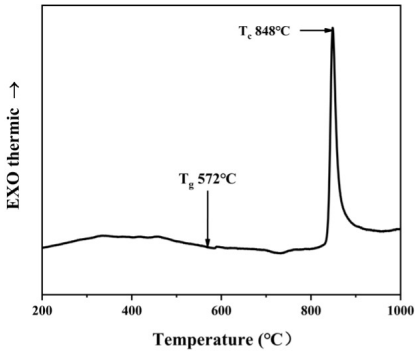

Figure 1. DSC of the parent glass with a heating rate of 10 °C·min^{-1}.

Structural analysis

XRD analysis of the glass-ceramics

The XRD of the glass-ceramics are presented in Figure 2. When the crystallisation temperature was 760 °C, the peak representing the glass phase appeared at 2θ = 10 – 30 °, indicating that there was no crystal or little crystal content in the glass at 760 °C. With an increasing crystallisation temperature, the XRD of the glass-ceramics began to show obvious diffraction peaks in the C-780 sample. The XRD patterns of the five samples were similar. It was noted that the crystal phase of all the samples was a hexagonal β-quartz solid solution ($Li_xAl_xSi_{1-x}O_2$, PDF Number: 25-8813). The crystallinity (R < 5 %) was calculated by the full spectrum fitting, the results are shown in Figure 3. The crystallinity and reference specific ratio of the samples were as follows: C-780 was 80.51 %, R = 4.21 %; C-800 was 82.97 %, R = 4.21 %; C-820 was 83.55 %, R = 3.84 %; C-840 was 83.69 %, R = 4.13 %; C-860 was 84.5 %, R = 4.72 %. It is generally believed that the lower the R value, the higher the calculation accuracy. It can be seen that the crystallinity increased from 80.51 % to 84.05 %, with an increase in the crystallisation temperature. It showed that the content of the β-quartz solid solution is continuously increasing.

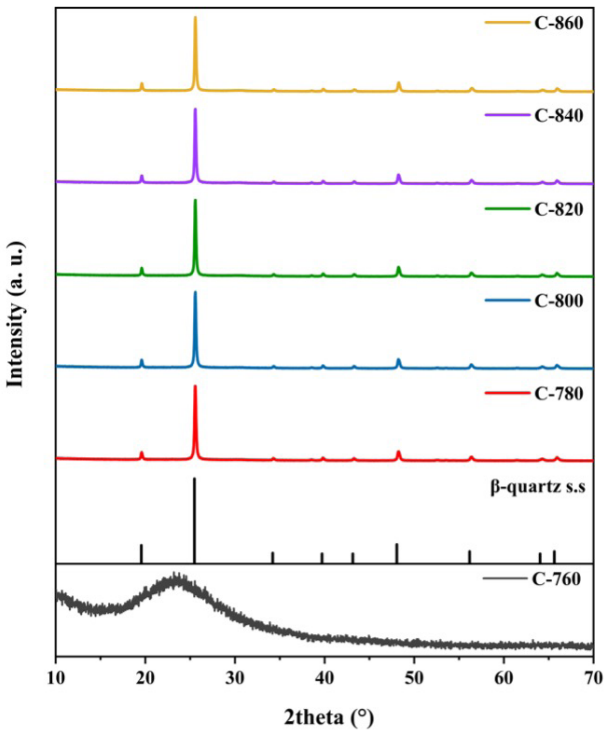

Figure 2. XRD pattern of the glass-ceramics.

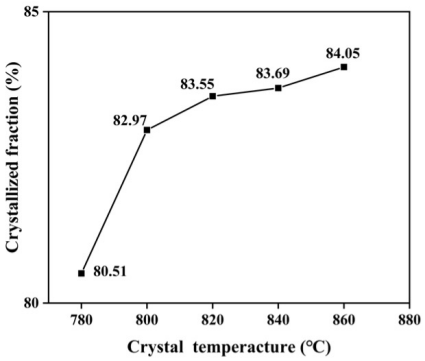

Figure 3. Crystallised fraction of the glass-ceramics (volume percentage).

SEM analysis of the glass-ceramics

The microstructure of the precipitated crystals is exhibited in Figure 4. It is noted that some nanoparticles were formed in the C-760 sample, which may be a part of the crystals. The XRD diffraction peak was a broad peak, which was attributed to the low crystal content. In this system, TiO_2 and ZrO_2 were the nucleating agents, many nanocrystals were formed during

the nucleation process [20]. TiO_2, ZrO_2 and $ZrTiO_4$ were first formed during the heat treatment process, and the crystals grew in the enrichment zone [14, 21, 22]. For the C-780 sample, the largest size of crystals of about 10 nm was observed. Most of the crystals were in contact with adjacent crystals because of the high crystallinity.

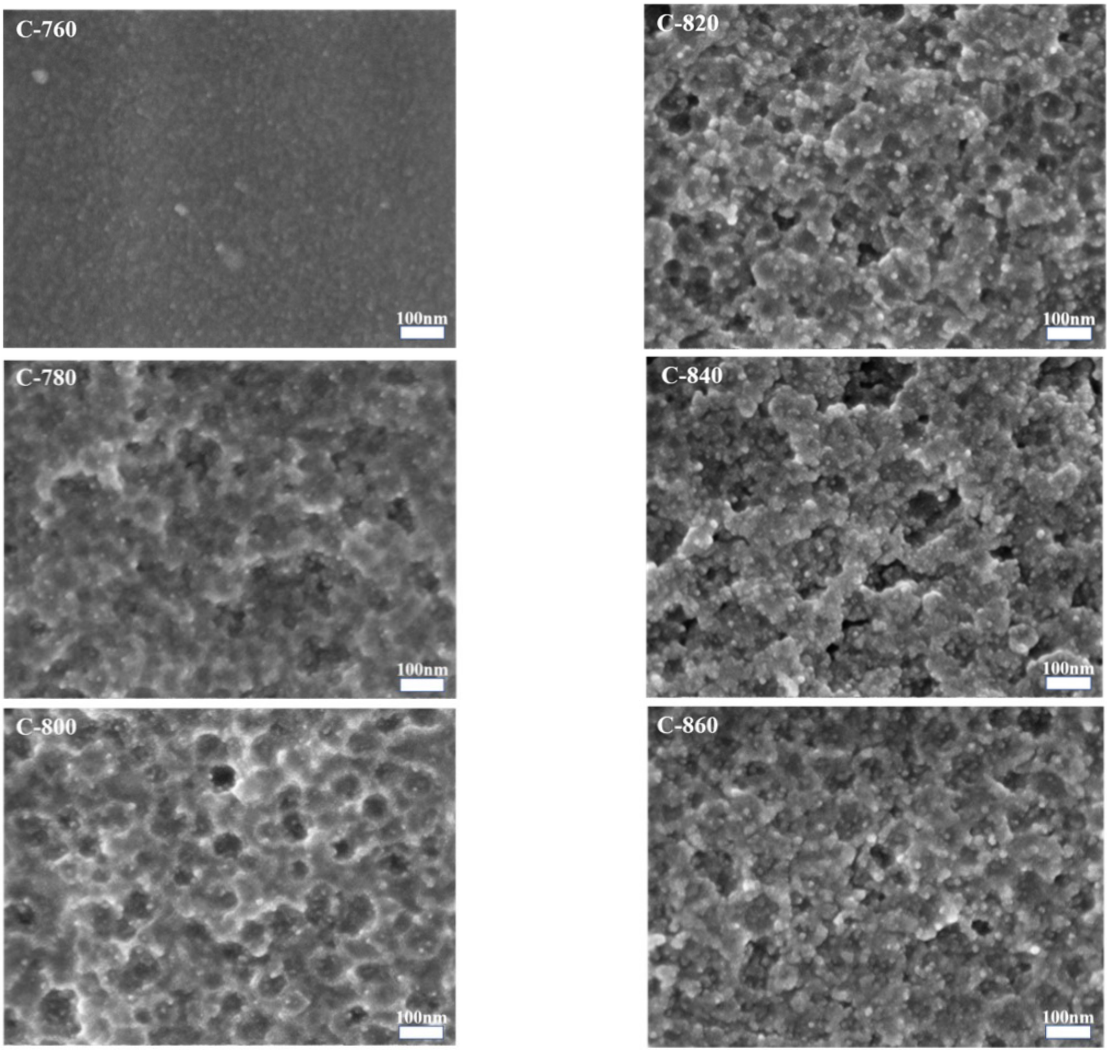

Figure 4. SEM of the glass-ceramics.

The grain size in the C-780 sample was uneven and presented a dispersed state. When increasing the crystallisation temperature, samples with a grain size about 10 – 20 nm were obtained, the remaining glass in the glass-ceramics became smaller, and the number of crystals increased significantly. According to the XRD results, Scherrer's equation can be used to calculate the average nanocrystal size.

Scherrer's equation:

$$D = \frac{K\lambda}{\beta \cos \theta} \quad (1)$$

where D is expressed as the average size of the nanocrystals; K is a constant (0.89); λ is the X-ray incidence wavelength (0.154 nm); β is the full-width at the half-maximum (FWHM) of the diffraction peak; θ is the diffraction angle [2]. The calculated average crystal sizes were 33.13 nm, 34.02 nm, 36.33 nm, 36.34 nm, and 36.81 nm for the C-780, C-800, C-820, and C-840 glass-ceramics samples, respectively. The calculated average crystal size is shown in Table 1. The values were shown to be different from the SEM results, because the formula calculates the size of the aggregate crystals, which is significantly larger than that observed microscopically [14]. The accumulation of crystal particles in the C-840 glass matrix increased the internal voids [13], a large number of voids in the glass phase were filled by the accumulation of precipitated crystals from the C-860 sample, and the arrangement and distribution were tighter than the previous samples [4]. The high Al_2O_3 content resulted in an increase in the

Table 1. The crystal grain size of the glass sample after the crystallisation treatment calculated by the XRD results.

Samples	C-780	C-800	C-820	C-840	C-860
Average size (nm)	33.13	34.02	36.33	36.34	36.56

viscosity of the glass, which made it more difficult for the particle diffusion [8]. The crystals tended to grow on the nuclei formed by TiO_2 and ZrO_2 rather than homogeneous nucleation because of the increase in the nucleation barrier. Therefore, the crystal distribution was more uniform. A conclusion can be drawn that the increasing crystallisation temperature was beneficial to form well-dispersed grains and for the well-regular arrangement.

FTIR analysis of the glass-ceramics

The structural changes of the parent glass and glass-ceramics were studied by FTIR in a range of 400 – 1600 cm^{-1}. In Figure 5, compared with the parent glass, new absorption bands near 542, 829, and 1024 cm^{-1} were observed in the glass-ceramics. Among them, the absorption band near 542 cm^{-1} was attributed to the in-plane bending vibration of Si-O-Al, and the band near 829 cm^{-1} was attributed to the symmetrical bending of Si-O-Si. The band near 1024 cm^{-1} originated from the asymmetrical flexural vibration of Si-O-Al. These new splitting vibrations were due to the precipitation of the β-quartz solid solution after the heat treatment of the glass. The glass-ceramics band shifted from a high wavenumber (462 cm^{-1}) to a low wavenumber (452 cm^{-1}), which was due to the distortion of [SiO_4] in the β-quartz solid solution [23]. Bands around 431, 542, 752, 829, 1021 and 1068 cm^{-1} were observed in all the glass-ceramics, and the strongest band was 700 – 900 cm^{-1}. The absorption groups corresponding to the infrared wave numbers are shown in Table. 2.

Table 2. Infrared vibration groups of the glass-ceramics.

Wave number (cm^{-1})	Characteristic vibration
1068	Asymmetric stretching vibration of Si-O-Si and Si-O-Al
1021	Asymmetric stretching vibration of Si-O-Al
752,725	Symmetrical stretching vibration of Si-O-Si and O-Si-O
542	Flexural vibration of Si-O-Al
462,452,431	Flexural vibration of Si-O-Si

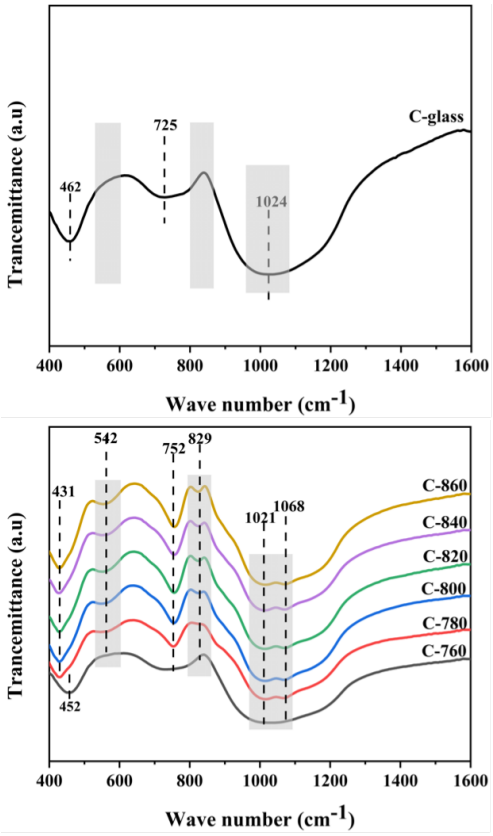

Figure 5. FTIR diagram of the parent glass (C-glass) and glass-ceramics (the grey area is the position of the new splitting absorption vibration peak).

In the β-quartz solid solution, the Al^{3+} replaced Si^{4+}, along with larger cationic voids occupied by Li^+, where the regular arrangement of the internal structure will be formed, which can strengthen the mutual vibration between the molecules and cause the band to move to low wave numbers (452 to 431 cm^{-1}). The [SiO_4] in the β-quartz solid solution was arranged in order, the Si-O-Si was more symmetrical, which narrows the internal bond length and bond angle, resulting in a higher band intensity and peak shape [24]. Therefore, the symmetrical structure in the crystal, the bond length distribution and the low angle between the bonds lead to sharp and strong absorption bands. The bands of 752 and 829 cm^{-1} became narrower, and a sharper trend was shown in the absorption peak band, which was related to the decrease in the silicate framework polymerisation of the glass. Glass-ceramics were easily crystallised due to the reduced stability of the glass network. The conclusion is that the increase in the crystallisation temperature was beneficial to the precipitation of the β-quartz solid solution.

Raman analysis of the glass-ceramics

The existence of or change in the internal structural units of the glass-ceramics was reflected by Raman spectroscopy. The Raman diagram of the glass-ceramics

is shown in Figure 6. The vibration peak of the bridging oxygen of the four-membered ring formed by the [SiO_4] tetrahedron [25] (D1 band) was near 481 cm-1. The vibration peak of 549 cm^{-1} indicated that there was a three-membered ring structure (D2 band) formed by the [SiO_4] tetrahedron in the glass-ceramics structure, corresponding to the three-membered ring containing one or more Si^{+} replaced by Al^{3+}. The D2 band obviously increased on the C-760 sample compared with the C-glass, indicating that part of the β-quartz solid solution was precipitated, which verified the SEM

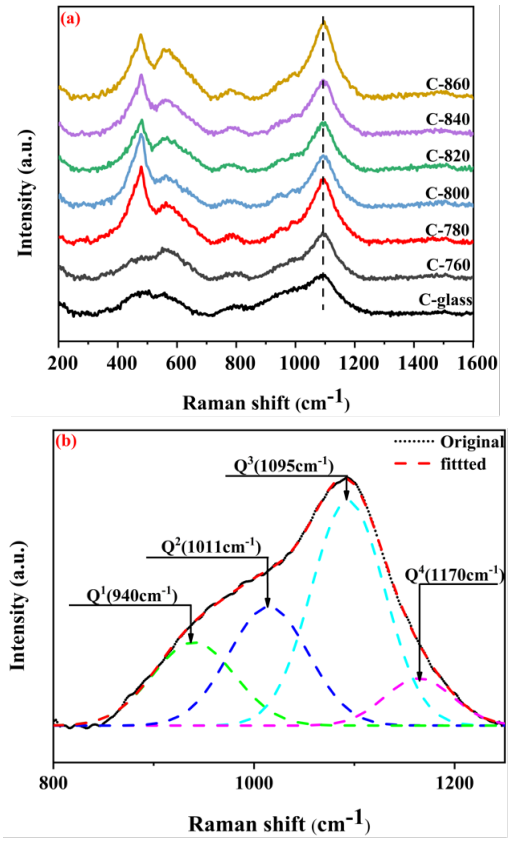

Figure 6. (a) Raman spectra of the parent glass and glass-ceramics, (b) Raman deconvolution results of the parent glass at 800 – 1250 cm^{-1} (R2 is greater than 0.99).

analysis. With an increasing crystallisation temperature, the band shifts of the glass-ceramics samples were increased at 481 cm^{-1} and 549 cm^{-1}. This was caused by the decrease in the Si-O-Si bond angle and the increase in the vibration frequency after the Al^{3+} replaced the Si^{4+} [26]. The peak kept narrowing and the intensity increased, and more Al^{3+} entered the glass network [27], which also corresponded to the increased precipitation of the β-quartz solid solution. The peaks of 850 – 1250 cm^{-1} corresponded to the vibration of the silicon-oxygen tetrahedron Q_n, which was caused by the tensile vibration of the end groups of the silicon-oxygen tetrahedron with different non-bridging oxygen atoms [28]. The number of bridging oxygen atoms was represented by n, a larger n represents a denser glass network [9]. It can be seen that the peak position was basically unchanged, and the peak intensity gradually rose with the increase in the crystallisation temperature. The deconvolution results of 800 – 1250 cm^{-1} of the parent glass are shown in Figure 6b. The main peak corresponds to Q_3. The increase in the peak intensity of the glass-ceramics was mainly due to the increase in the Q_3, which was also related to the precipitation of the β-quartz solid solution [25]. This showed that the increasing temperature was beneficial to the precipitation of the β-quartz solid solution, which was consistent with the FTIR analysis.

Performance analysis

The linear CTE of the LAS glass-ceramics is mainly determined by the content of the β-quartz solid solution crystals. The β-quartz solid solution is composed of an [AlO_4] tetrahedron and an [SiO_4] tetrahedron. The vertices of these two tetrahedrons are connected together through O atoms to form a ring structure [24, 29, 30]. At a high temperature, the repulsive force between the ions in the crystal reduced due to the expansion of the ions in the xy plane. In order to maintain the stability of the Li-O bond and the tetrahedron in the crystal, the crystal network shrinks along the c-axis direction, and the strong negative expansion at c is presented in the c-axis direction [24]. This is the reason for the low thermal expansion of the β-quartz solid solution.

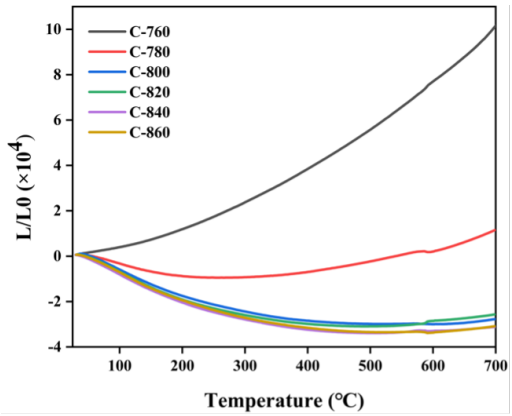

Figure 7. CTE of glass-ceramics.

The CTE of the glass-ceramics is exhibited in Figure 7. The thermal expansion of the C-760 sample was positive and lower than the parent glass, which further showed that the β-quartz solid solution was precipitated at the crystallisation temperature of 760 °C.

The CTE in the C-780 sample approached zero expansion, the positive expansion of the glass phase was offset by the negative expansion of the precipitated β-quartz solid solution, making the sample to have close to zero expansion. From the C-800 to C-860, the samples showed negative expansion and the thermal expansion curves were relatively familiar, indicating that the number of β-quartz solid solution crystals precipitated inside the glass-ceramics increased with an increase in the crystallisation temperature. When the crystallisation temperature was higher, the crystal content tended to stabilise. The average CTE is shown in Figure 8.

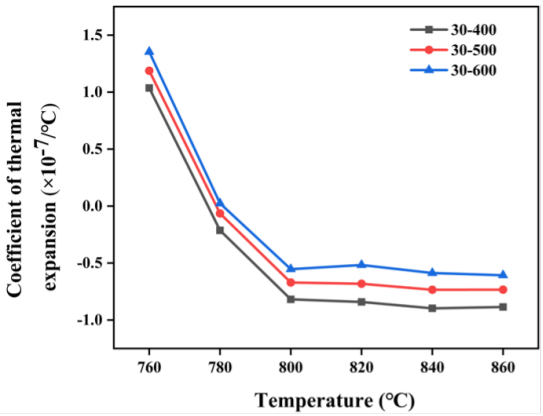

Figure 8. Changes in the average CTE of the glass-ceramics.

samples are displayed in Figure 9. These samples have high transmittance in the visible light band. In the ultraviolet range, all the samples have strong absorption. The ultraviolet absorption of the glass-ceramics is related to the amount of bridging oxygen in the residual glass phase, the lower the bridging oxygen, the more the absorption limit wavelength increases [14]. It showed that an increased crystallisation temperature reduces the degree of polymerisation of the glass network, where the number of bridging oxygen atoms are decreased in the residual glass phase. This is consistent with FTIR and Raman results. With an increasing crystallisation

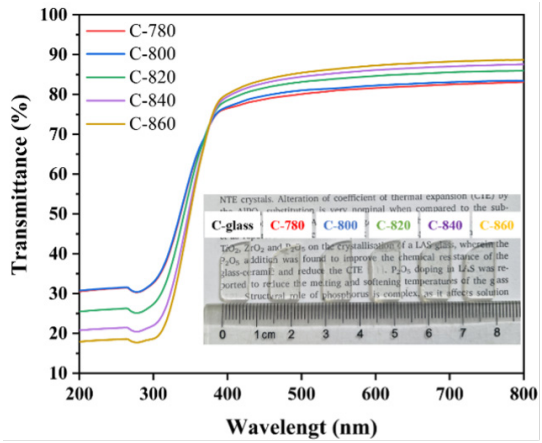

Figure 9. Transmittance spectra and photograph of the glass-ceramics (thickness of 2 mm).

Table 3. The CET of the glass-ceramics in different temperature ranges (10^{-7}).

Temperature (°C)	C-glass	C-760	C-780	C-800	C-820	C-840	C-860
30 – 400	4.943	1.035	-0.213	-0.818	-0.841	-0.897	-0.885
30 – 500	5.102	1.187	-0.065	-0.671	-0.680	-0.734	-0.730
30 – 600	5.113	1.353	0.023	-0.554	-0.517	-0.587	-0.607
30 – 700	5.297	1.522	0.164	-0.436	-0.395	-0.470	-0.471

As the temperature increased, the average CTE decreased. The average CTE of the 800 – 860 °C samples were all negative. According to the XRD analysis, there was no obvious increase in the crystal content, which was the reason why the CTE remained stable. The thermal expansion performance of the glass-ceramics was stable, which is of great significance for applications in cookware and in other areas.

According to the Rayleigh-Ganz scattering theory, the main factor affecting the transmittance is the crystal size [30]. The Rayleigh–Ganz–Debye light-scattering [31] showed that if crystal grain size further reduces to a nanometre level, the transmittance of transparent glass-ceramics will be greatly improved.

The transmittance in the visible light range (380 – 780 nm) and a photograph of the glass-ceramic

temperature, the visible light transmittance of the samples successively increased, and the highest was 88 % in the C-860 sample. The transmittance of the glass-ceramics in the visible light range were greater than 82 % in the C-780 sample. The increase in the transmittance was due to the precipitation of the nanocrystals and the size was less than 40 nm, it can be seen that the grain voids gradually decrease with an increase in the temperature as seen in the SEM. The transmittance slightly increased with the grain size which may be due to the increase in the number of scattering sources due to the decrease in the grain boundary fraction [32]. According to the SEM analysis, the increase in the crystallisation temperature was beneficial to the uniform distribution grains in the glass-ceramics, the uniformly arranged grains showed lower light scattering loss, the optical

transparency was higher, so that the light transmittance of the samples improved [30, 33].

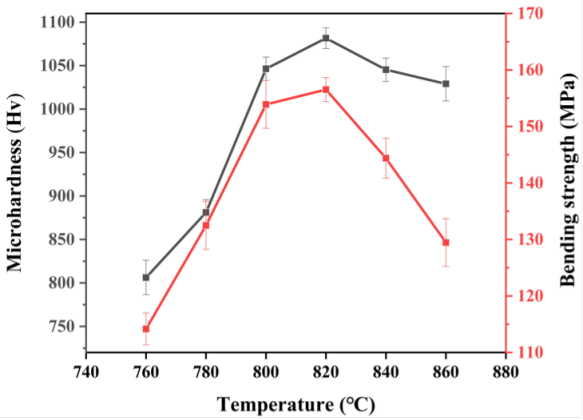

Figure 10. Mechanical properties of the glass-ceramics.

The ability of the material to resist external pressure is reflected by the bending strength, and the resistance of the material to deformation is reflected by the hardness [34]. The mechanical properties of the glass-ceramic samples at different crystallization temperatures are presented in Figure 10. With an increasing crystallisation temperature, the same trend in the changes was shown in the bending strength and microhardness, which initially increased to the maximum and then decreased. It was noted that the bending strength of the glass-ceramics was enhanced from 115 to 156 MPa and then decreased to 130 MPa and the microhardness increased from 820 to 1082 HV and then decreased to 1025 HV with the increasing crystallisation temperature. The maximum values all appeared in the C-820 sample, which were 156 MPa and 1082.09 HV, respectively. It can be explained for these aspects: when the crystallisation temperature was 760 °C, fewer crystals precipitated, and the ability to resist the external stress was weak, so the bending strength was lower. With an increasing crystallisation temperature, the amount of the β-quartz solid solution precipitated increased. The increase in the crystals can better prevent cracking and bending fractures, thus the bending strength was consequently improved [35]. The dislocation mobility was limited to the smaller β-quartz solid solution, and the number of crystals led to an increase in the hardness [33]. Starting from C-820, it can be seen that the bending strength and microhardness both showed a downward trend. In some areas of the glass-ceramics, it was difficult to improve the mechanical properties due to the obvious growth stress of the crystal compaction [36]. On the one hand, as the temperature increased, a large number of fine crystals were precipitated. The content of the grain boundaries in the glass-ceramic structure increased. The non-concentration of stress between the different grain boundaries led to the appearance of a lot of micro-holes and internal cracks, resulting in a decrease in the mechanical strength [21]. On the other hand, the glass phase was not sufficiently connected to the crystals. After being subjected to external forces, the ability to resist external forces decreases, which led to a decrease in the mechanical strength.

CONCLUSIONS

The effect of the crystallisation temperature on the crystallisation behaviour, structure, and properties of LAS glass-ceramics with a high Al_2O_3 content was investigated in this paper. The main conclusions are summarised as follows.

(1) When the crystallisation temperature ranged from 760 to 860 °C, the precipitation of a β-quartz solid solution was promoted. In addition, the size of the crystals inside the samples were all less than 20 nm, and the crystal phase was mainly composed of Q_3 structure units.

(2) The CTE of the glass-ceramics showed a negative correlation with the crystallisation temperature, while the visible light transmittance demonstrated a positive one. Moreover, as the temperature changed from 760 to 860 °C, the bending strength and microhardness of the glass-ceramics showed a tendency to first increase and then decrease.

(3) As the crystallisation temperature was 820 °C, the bending resistance and microhardness of the glass-ceramics reached the maximum, 156 MPa and 1082.09 HV, respectively. At the same time, the CTE of this sample was -0.395×10^{-7} K^{-1} in the range of 30 – 700 °C, and the visible light transmittance was 85 %.

Acknowledgment

This work was supported by research fund of Center for Materials Research and Analysis, Wuhan University of Technology (2018KFJJ11). The authors express their sincere gratitude to the Material Research and Testing Center of Wuhan University of Technology.

REFERENCES

1. Mahmoud M. M., Folz D. C., Suchicital C. T., Clark D. E. (2015): Estimate of the crystallization volume fraction in lithium disilicate glass-ceramics using Fourier transform infrared reflectance spectroscopy. *Journal of the European Ceramic Society, 35*(2), 597-604. Doi:10.1016/j.jeurceramsoc.2014.09.004
2. Zhao Y., Zhou B., Qiu P., Fan Y., Zheng Q., Luo W., Cheng X., Wang L., Jiang W. (2021): Ultra-low temperature preparation of mullite glass-ceramics with high transparency sintered from EMT-type zeolite. *Journal of the American Ceramic Society, 104*, 3158-3166. Doi:10.1111/jace.17751

3. Armistead W. H., Stookey S. D (1964): Photochromic Silicate Glasses Sensitized by Silver Halides. *Science, 144*, 150-154. Doi: 10.1126/science.144.3615.150
4. Al-Harbi O. A. (2009): Effect of different nucleation catalysts on the crystallization of Li2O-ZnO-MgO-Al2O3-SiO2 glasses. *Ceramics International, 35*, 1121-1128. Doi:10.1016/j.ceramint.2008.05.008
5. Zocca A., Gomes C. M., Bernardo E., Müller R., Günster J., Colombo P. (2013): LAS glass-ceramic scaffolds by three-dimensional printing. *Journal of the European Ceramic Society, 33*, 1525-1533. Doi: 10.1016/j.jeurceramsoc.2012.12.012
6. Beall G. H., Pinckney L. R (1999): Nanophase-glass-ceramics. *Journal of the American Ceramic Society, 82*, 5-16. Doi: 10.1111/j.1151-2916.1999.tb01716.x
7. Venkateswaran C., Sharma S. C., Pant B., Chauhan V. S., Vaish R. (2019): Crystallisation studies on site saturated lithium aluminosilicate (LAS) glass. *Thermochimica Acta, 679*, 178311. Doi:10.1016/j.tca.2019.178311
8. Soares V. O., Peitl O., Zanotto E. D., Pinckney L. (2013): New Sintered Li_2O-Al_2O_3-SiO_2 Ultra-Low Expansion Glass-Ceramic. *Journal of the American Ceramic Society, 96*, 1143-1149. Doi:10.1111/jace.12266
9. Zhou Z., He F., Shi M., Xie J., Wan P., Cao D., Zhang B.(2022): Influences of Al2O3 content on crystallization and physical properties of LAS glass-ceramics prepared from spodumene. *Journal of Non-Crystalline Solids, 576*, 121256. Doi:10.1016/j.jnoncrysol.2021.121256
10. Ren Q., Liu C., Zhang Q., Ouyang Y., Lu A.(2021): Effects of B_2O_3 substitution for Al_2O_3 on the crystallization and properties of translucent mica glass-ceramics. *Journal of the European Ceramic Society, 41*, 334-341. Doi:10.1111/ijag.15904
11. Karmakar B., Kundu P., Jana S., Dwivedi R. N. (2002): Crystallization Kinetics and Mechanism of Low-Expansion Lithium Aluminosilicate Glass-Ceramics by Dilatometry. *Journal of the American Ceramic Society, 85*, 2572-2574. Doi:10.1111/j.1151-2916.2002.tb00498.x
12. Sun Y., Ma L., Cui J., Feng L., Zhang Z., Yang Y., Han N., Zhang W., Sun Q., Cao X., Wang T. (2021): Effects of heat-treatment temperature and holding time on the microstructure and mechanical properties of lithium disilicate glass-ceramics. *Journal of Non-Crystalline Solids, 553*, 120502. Doi:10.1016/j.jnoncrysol.2020.120502
13. Kumar A., Chakrabarti A., Shekhawat M. S., Molla A. R. (2019): Transparent ultra-low expansion lithium aluminosilicate glass-ceramics: Crystallization kinetics, structural and optical properties. *Thermochimica Acta, 676*, 155-163. Doi:10.1016/j.tca.2019.04.006
14. Zhang R., Yi L., Kong F., Liang X., Yin Z., Rao Y., Wang D., Chen Z., Yu X., Jiang H., Li C. (2021): Rapid preparation of low thermal expansion transparent LAS nanocrystalline glass by one-step thermoelectric treatment. *Ceramics International, 47*, 34380-34387. Doi: 10.1016/j.ceramint.2021.08.350
15. Kim K. D., Lee S. H., Hwang J. H., Seo W. S. (2007): Nucleation behavior and microstructure of Al_2O_3-poor LAS glass-ceramics. *Journal of Materials Science, 42*, 10180-10187. Doi:10.1007/s10853-007-1983-1
16. Lee D., Joo S. H., Shin D. J., Shin S. M. (2021): Evaluation of leaching characteristic and kinetic study of lithium from lithium aluminum silicate glass-ceramics by NaOH. *Journal of Environmental Sciences, 107*, 98-110. Doi:10.1016/j.jes.2021.02.001
17. Nnakwo K. C., Amadi F. E., Mbah C. N. (2019): Influence of heat treatment regimes on crystalline phase formation and physical properties of Li_2O-SiO_2-Al_2O_3 glass system. *Materials Research Express, 6*, 095202. Doi:10.1088/2053-1591/ab2c25
18. Li T., Wang J., Ruan J., Liu C., Han J. (2021): Crystallization behavior of transparent Na_2O-Al_2O_3-SiO_2 glass-ceramic containing rare-earth oxides. *Journal of Non-Crystalline Solids, 567*, 120935. Doi:10.1016/j.jnoncrysol.2021.120935
19. Karan R., Pal P., Maiti P. K., Das K.(2021): Structure, properties and in-vitro response of SiO_2-Na_2O-CaO-P_2O_5 system based glass-ceramics after partial replacement of Na_2O by Li_2O. *Journal of Non-Crystalline Solids, 556*, 20554. Doi:10.1016/j.jnoncrysol.2020.120554
20. Guo X., Yang H., Cao M.(2005): Nucleation and crystallization behavior of Li_2O-Al_2O_3-SiO_2 system glass-ceramic containing little fluorine and no-fluorine. *Journal of Non-Crystalline Solids, 351*, 2133-2137. Doi:10.1016/j.jnoncrysol.2005.04.071
21. Wu J., Lin C., Liu J., Han L., Gui H., Li C., Liu T., Lu A.(2019): The effect of complex nucleating agent on the crystallization, phase formation and performances in lithium aluminum silicate (LAS) glasses. *Journal of Non-Crystalline Solids, 521*, 119486. Doi:10.1016/j.jnoncrysol.2019.119486
22. Chavoutier M., Caurant D., Majérus O., Boulesteix R., Loiseau P., Jousseaume C., Brunet E., Lecomte E.(2014): Effect of TiO_2 content on the crystallization and the color of (ZrO_2,TiO_2)-doped Li_2O-Al_2O_3-SiO_2 glasses. *Journal of Non-Crystalline Solids, 384*, 15-24. Doi:10.1016/j.jnoncrysol.2013.03.034
23. Li Y., Liang K., Cao J., Xu B.(2010): Spectroscopy and structural state of V^{4+} ions in lithium aluminosilicate glass and glass-ceramics. *Journal of Non-Crystalline Solids, 356*, 502-508. Doi:10.1016/j.jnoncrysol.2009.12.018
24. Chen M., He F., Shi J., Xie J., Yang H., Wan P. Wan.(2019): Low Li_2O content study in Li_2O-Al_2O_3-SiO_2 glass-ceramics. *Journal of the European Ceramic Society, 39*, 4988-4995. Doi:10.1016/j.jeurceramsoc.2019.07.032
25. Paul McMillan t A. P., Carpenter M. A.(1984): A Raman Spectroscopic Study of Al-Si Ordering in Synthetic Magnesium Cordierite. *Physics and Chemistry of Minerals, 10*, 256-260.Doi:10.1007/BF00311950
26. Alekseeva I., Dymshits O., Ermakov V., Zhilin A., Petrov V., Tsenter M.(2008): Raman spectroscopy quantifying the composition of stuffed β-quartz derivative phases in lithium aluminosilicate glass-ceramics. *Journal of Non-Crystalline Solids, 354*, 4932-4939. Doi:10.1016/j.jnoncrysol.2008.07.016
27. Bechgaard T. K., Goel A., Youngman R. E., Mauro J. C.,

Rzoska S. J., Bockowski M., Jensen L. R., Smedskjaer M. M. (2016): Structure and mechanical properties of compressed sodium aluminosilicate glasses: Role of non-bridging oxygens. *Journal of Non-Crystalline Solids, 441*, 49-57. Doi:10.1063/1.4882283

28. Koroleva O. N., Shabunina L. A., Bykov V. N. (2011): structure of borosilicate glass according to raman spectroscopy data. *Glass and Ceramics, 67*, 11-12. Doi:10.1007/s10717-011-9293-0
29. L. Arnault M. G., `Ere A. R.(2000): Microstructural study of two LAS-type glass-ceramics and their parent glass. *Journal of Material Science, 35*, 2331-2345. Doi:10.1023/A:1004716018522
30. Zandona A., Helsch G., Deubener J. (2020): Deubener, Inversion of quartz solid solutions at cryogenic temperatures. *Journal of the American Ceramic Society, 103*, 6630-6638. Doi:10.1111/jace.17393
31. Apetz R., Van Bruggen M. P. (2003): Transparent alumina: a light-scattering model. *Journal of the American Ceramic Society, 86*(3), 480-486. Doi: 10.1111/j.1151-2916.2003.tb03325.x
32. Wang P., Huang Z., Morita K., Li Q., Yang M., Zhang S., Goto T., Tu R.(2021): Transmittance enhancement of spark plasma sintered CaF_2 ceramics by preheating commercial powder. *Journal of the European Ceramic Society, 41*, 4609-4617. Doi:10.1016/j.jeurceramsoc.2021.03.014
33. Lallemant L., Garnier V., Bonnefont G., Marouani A., Fantozzi G., Bouaouadja N.(2014): Effect of solid particle impact on light transmission of transparent ceramics: Role of the microstructure. *Optical Materials, 37*, 352-357. Doi:10.1016/j.optmat.2014.06.025
34. Aliyah L. H., Katrina A. T., Hasmaliza M. (2019): Preliminary study on the development of new composition lithium aluminosilicate glass ceramic. *Materials Today: Proceedings, 17*, 946-952. Doi:10.1016/j.matpr.2019.06.446
35. al A. J. K. e. (1995): Fracture Mechanics. Springer Science + Business Media Dordrecht 75-106. 2nd ed. CRC Press.
36. Aliyah L. H., Izzat B. M., Hasmaliza M., Katrina A. T. (2020): Effect of mechanical properties on sintered lithium aluminosilicate glass ceramic and its thermal shock resistance properties. *AIP Conference Proceedings, 2267*, 020047.
37. Ananthanarayanan A., Kothiyal G. P., Montagne L., Revel B. (2010): MAS-NMR studies of lithium aluminum silicate (LAS) glasses and glass–ceramics having different Li_2O/Al_2O_3 ratio. *Journal of Solid State Chemistry, 183*(1), 120-127. Doi: 10.1016/j.jssc.2009.10.006
38. Beall G. H., Duke D. A. (1969): Transparent glass-ceramics. *Journal of Materials Science, 4*(4), 340-352. Doi: 10.1007/BF00550404
39. Wu J., Lin C., Liu J., Han L., Gui H., Li, C., et al. (2019): The effect of complex nucleating agent on the crystallization, phase formation and performances in lithium aluminum silicate (LAS) glasses. *Journal of Non-Crystalline Solids, 521*, 119486. Doi: 10.1016/j.jnoncrysol.2019.119486.